

DAG: Depth-Aware Guidance with Denoising Diffusion Probabilistic Models

Gyeongnyeon Kim*, Wooseok Jang*, Gyuseong Lee*, Susung Hong, Junyoung Seo, Seungryong Kim†
Korea University, Seoul, Korea

{kkn9975, jws1997, jpl358, susung1999, se780, seungryong_kim}@korea.ac.kr

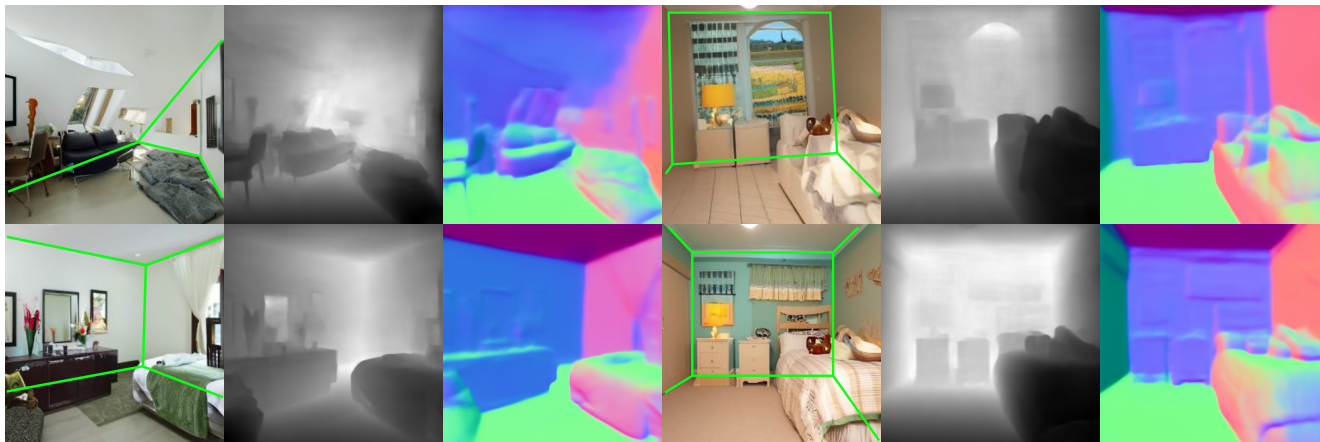


Figure 1. **Qualitative comparisons of synthesized images without guidance [8] (top) and with our depth-aware guidance (DAG), and their corresponding estimated depths [39] and surface normals [3].** Note that we highlight the scene layouts on the generated images. Our DAG helps better generate geometrically plausible images compared to the baseline [8].

Abstract

In recent years, generative models have undergone significant advancement due to the success of diffusion models. The success of these models is often attributed to their use of guidance techniques, such as classifier and classifier-free methods, which provides effective mechanisms to trade-off between fidelity and diversity. However, these methods are not capable of guiding a generated image to be aware of its geometric configuration, e.g., depth, which hinders the application of diffusion models to areas that require a certain level of depth awareness. To address this limitation, we propose a novel guidance approach for diffusion models that uses estimated depth information derived from the rich intermediate representations of diffusion models. To do this, we first present a label-efficient depth estimation framework using the internal representations of diffusion models. At the sampling phase, we utilize two guidance techniques to self-condition the generated image using the estimated depth map, the first of which uses pseudo-labeling, and the subsequent one uses a depth-domain diffusion prior. Experiments and exten-

sive ablation studies demonstrate the effectiveness of our method in guiding the diffusion models toward geometrically plausible image generation. Project page is available at <https://ku-cvlab.github.io/DAG/>.

1. Introduction

Diffusion models [20, 37, 40, 50] have recently received much attention and have shown remarkable generation quality. Such superior performance of diffusion models promoted many applications, such as text-guided image synthesis [36, 38], image restoration [23, 42, 44] and semantic segmentation [1, 4].

Generally, generative models [12, 16, 20], including diffusion models, focus primarily on visual texture, e.g., realistic appearance, but hardly consider shape geometry during the image generation process. As a result, as demonstrated in Fig. 1, conventional diffusion models often generate geometrically implausible images that contain ambiguous depth and cluttered object layouts. These synthesized samples with such unrealistic 3D geometry, whose deviation can be effectively captured by the depth map in 2D, are problematic in that they are not only visually unappealing

* Authors contributed equally.

† Corresponding author.

but also unsuitable for downstream tasks, e.g., robotics and autonomous driving [55, 63].

While there have been some class-conditional guidance approaches [8, 21] that drive the sampling process of diffusion models to a class-specific distribution, it has rarely been researched to guide the sampling process toward a depth-specific distribution. This motivates us to propose a novel framework, called Depth-Aware Guidance (DAG), that can introduce depth awareness to diffusion models. Training diffusion models or depth predictors from scratch with depth-image pairs, as in conventional guidance, [8, 21] can be challenging because it requires a lot of effort to annotate the ground-truth depth map and it takes tremendous time and computations to jointly train the models. Therefore, we train the depth predictors for the first time by exploiting rich representations of a pretrained diffusion model. This is based on our careful analysis of the representational power of the U-Net of diffusion models with respect to the depth prediction tasks.

Furthermore, leveraging label-efficient depth predictors, we propose a novel depth-aware guidance approach for image generation with the diffusion model. Our approach mainly demonstrates two guidance strategies that effectively guide the image’s geometric awareness: depth consistency guidance and depth prior guidance. The first strategy, depth consistency guidance, is motivated by consistency regularization [2, 28, 45], which is one of the most commonly and widely used strategies for semi-supervised learning. By treating the better prediction as a pseudo-label, depth consistency guidance guides the image toward improving the poor prediction. For depth prior guidance, we leverage the fact that an additionally pretrained diffusion U-Net can be used as a prior network [17] to provide guidance during the sampling process. Through this design, we explicitly inject depth information into the sampling processes of diffusion models. To the best of our knowledge, our work is the first attempt to not only propose a simple depth estimation with representations of diffusion models but also utilize depth information during the sampling process to make image generation more geometrically consistent.

In the experiments, we evaluate our methods on challenging indoor scene datasets [35, 64]. We conduct extensive ablation studies to validate our approach. Also, we propose new metrics for evaluation, from the perspective of depth estimation task since well-known existing metrics such as FID [19] or Inception Score [46] are not suitable for capturing geometric awareness. The sufficient superiority of our method is demonstrated in both qualitative and quantitative results.

To sum up, we present the following key contributions:

- For the first time, we investigate the depth information contained in the learned U-Net representations of diffusion models.

- Based on the investigation, we propose a novel framework that can impose depth awareness of images generated from diffusion models.
- The training of depth predictors in this framework can be done in a label-efficient manner by piggybacking on pretrained diffusion models.
- We propose novel guidance strategies that make use of consistency regularization and depth prior.

2. Related Work

Denoising diffusion probabilistic models. Diffusion models [20, 50], as the name states, model the reverse diffusion process, which gradually removes Gaussian noise from the latent variable. [53] have shown that diffusion models are equivalent to score-based generative models via stochastic differential equation interpretation. These models allow us to generate images from a complete Gaussian noise. Many attempts have been made to improve the sample quality and sampling speed through various approaches [8, 22, 37, 40, 52]. [37] estimated the variance of reverse diffusion process and [8] searched for an optimal U-shaped architecture for better sampling quality. [52] proposed non-Markovian diffusion process to reduce sampling steps whereas [40] leveraged diffusion process in the discrete latent space introduced in [11] for efficient computation and faster sampling. As a result of this remarkable research, diffusion models now outperform previous state-of-the-art models in various image generation tasks [7, 36, 38, 40, 43, 47].

Sampling guidance for diffusion models. [8] first proposed classifier guidance that leverages the gradient of an external classifier during the sampling process. By scaling the gradient, we can control the trade-off between the fidelity and diversity of the generated images. As an alternative without needing an external classifier, classifier-free guidance [21] has been proposed. During training, they randomly drop a certain percentage of class labels to obtain both conditional and unconditional models with shared parameters. With these two models, they get a similar effect on the classifier guidance. Applying these guidance leads to significant development in a conditional generation like text-to-image generation [18, 36, 38, 40, 43] and semantic map-guided image generation [60, 61]. However, to our best knowledge, no research utilizes the guidance for sampling with geometric awareness.

Internal representations in diffusion models. Recently, several works [1, 4] have analyzed and utilized the intermediate U-Net representations of diffusion models. [4] conducted various semantic analyses about the U-Net representations of diffusion models at different layers. The work demonstrated that the U-Net [4] representations contain

some semantic contexts of images so that they can predict a semantic segmentation map only using a shallow MLP and scarcely-labeled dataset. Also, [1] found similar phenomena that decoder pretraining of recovering the noised image like denoising autoencoders [58] achieves high performance in label-efficient semantic segmentation task. For the first time, we propose to capture depth information using internal representations.

Monocular depth estimation. Monocular depth estimation, which aims to estimate a dense depth map from a single image [10, 24, 31, 56, 62], is an essential component of 3D perception. Since [10] proposed a deep learning-based approach for this task, several works [13, 27, 30] have achieved significant progress due to the ability of CNNs to learn strong priors from images corresponding to the geometric layout. Following the recent success of Transformer [9, 57] in vision tasks, [5, 32, 39] employed a Transformer-based encoder to exploit a global receptive field. Despite notable improvements, recent works increase the model complexity and the reliance on large paired supervision.

3. Preliminaries

Denoising diffusion probabilistic models. DDPM [20] is a kind of generative model that generates an image by iteratively denoising from Gaussian noise. In specific, given an input image \mathbf{x}_0 and an input noise $\epsilon \sim \mathcal{N}(\mathbf{0}, \mathbf{I})$, DDPM gradually adds noise according to a timestep t . For a pre-defined variance schedule β_t for $t \in \{T, T-1, \dots, 1\}$, we denote α_t and $\bar{\alpha}_t$ as $1 - \beta_t$ and $\prod_{k=1}^t \alpha_k$, respectively. Then, given an arbitrary t , the forward process can be expressed as a closed form [20]:

$$\mathbf{x}_t = \sqrt{\bar{\alpha}_t} \mathbf{x}_0 + \sqrt{1 - \bar{\alpha}_t} \epsilon. \quad (1)$$

As noted in Ho et al. [20], we can re-weight the training objective of DDPM as:

$$\mathcal{L}_{\text{simple}} = \|\epsilon - \epsilon_\theta(\mathbf{x}_t)\|_2^2, \quad (2)$$

where ϵ_θ is a denoising U-Net [20] parameterized with θ . Subsequently, the sampling process of DDPM is defined as the reverse of the forward process:

$$\mathbf{x}_{t-1} \sim \mathcal{N}(\mu_\theta(\mathbf{x}_t), \sigma_t^2), \quad (3)$$

where σ_t^2 is a constant only dependent on t , and μ_θ is a prediction of the mean computed from the reparameterization of ϵ_θ . In some works [8, 37], the variance is also predicted and then Eq. 3 turns into:

$$\mathbf{x}_{t-1} \sim \mathcal{N}(\mu_\theta(\mathbf{x}_t), \Sigma_\theta(\mathbf{x}_t)), \quad (4)$$

where Σ_θ is a prediction of variance in the reverse process from the model output. To formulate the task as conditional image generation with diffusion models, the need for guidance method is increasing.

Classifier guidance for diffusion model. By providing a way to trade off diversity and fidelity, classifier guidance [8] can improve the sample quality for image synthesis tasks. For a trained classifier $p_\psi(\mathbf{y}|\mathbf{x}_t)$ that receives the noised image \mathbf{x}_t and predicts the class \mathbf{y} , a gradient with respect to \mathbf{x}_t is calculated as:

$$\nabla_{\mathbf{x}_t} \log(p_\psi(\mathbf{y}|\mathbf{x}_t)). \quad (5)$$

Then, the sampling process with classifier guidance is defined as follows:

$$\mathbf{x}_{t-1} \sim \mathcal{N}(\mu_\theta(\mathbf{x}_t) + w \Sigma \nabla_{\mathbf{x}_t} \log(p_\psi(\mathbf{y}|\mathbf{x}_t)), \Sigma_\theta(\mathbf{x}_t)). \quad (6)$$

where $w > 0$ is a scale of guidance.

Even though this technique improves the sampling quality, no studies have attempted to extend it by leveraging dense predictors that incorporate geometric awareness.

4. Methodology

4.1. Motivation and Overview

Although the synthesized images by existing generative models such as GANs [15] or diffusion models [20, 50] seem to be fairly plausible, they often fail to incorporate geometric awareness. For example, the generated images by the existing models [12] often contain out-of-perspective or distortion of the layout, as depicted in Fig. 1. This failure of considering geometric awareness can be an obstacle when applied to many downstream tasks [33, 55], which require geometrically realistic images.

To overcome this, we propose a novel framework (see Fig. 2) to explicitly incorporate geometric information into the diffusion model as guidance. Specifically, to generate depth-aware images, we first train depth predictors using internal representation [4] with a small amount of depth-labeled data. Then, we guide the intermediate images using obtained depth map in the sampling process.

In the following, in Sec. 4.2, we demonstrate a way to acquire a depth map in a label-efficient way, and in Sec. 4.3, we propose sampling methods to guide the generated images to have depth awareness.

4.2. Label-Efficient Training of Depth Predictors

In order to generate depth-aware images with diffusion guidance in a straightforward way as in [8], we need either a large amount of image-depth pairs or an external large-scale depth estimation network trained on the noised images, both of which are challenging to acquire. To address this problem, we re-use the rich representations learned with DDPM that may contain depth information of images to estimate the depth.

Network architecture. Recent research has shown that the internal features of the networks trained with diffusion

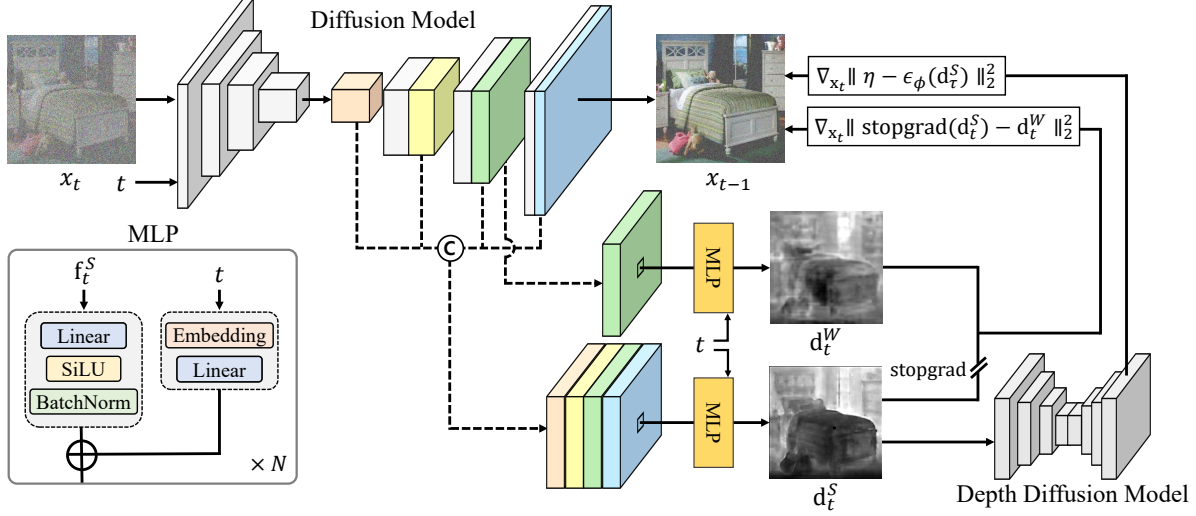


Figure 2. **Overview of our framework.** First of all, we train asymmetric pixel-wise depth predictor conditioned on a timestep with respect to pretrained diffusion models in a label-efficient manner. Then, we apply two guidance strategies. First, we extract strong and weak depth maps with this predictor from DDPM network and give a depth consistency guidance. Next, giving the depth map from the strong branch as an input, the pretrained depth diffusion model is utilized to push the model prior into intermediate images to be depth-aware.

models can encode semantic information [1, 4, 58], and our contribution builds upon this by incorporating depth information into the framework.

To perform depth estimation in a label-efficient manner, we utilize a pixel-wise shallow Multi-Layer Perceptron (MLP) regressor that receives intermediate features from U-Net and estimates the depth values of the noisy input image. Specifically, we acquire the internal features $\mathbf{f}_t(k) \in \mathbb{R}^{C(k) \times H(k) \times W(k)}$ from the output of k -th decoder layer in the diffusion U-Net, where $C(k)$ denotes the channel dimension and $H(k) \times W(k)$ denotes the spatial resolution of the k -th layer of the U-Net decoder. Subsequently, we form the depth map by querying the MLP blocks pixel-by-pixel, where the depth map can be formulated as:

$$\mathbf{d}_t(k) = \text{MLP}(\mathbf{f}_t(k)). \quad (7)$$

Also, similar to [4], it is generally better to use more features from different U-Net layers than only using the feature from one layer. Therefore we extract more features from many layers and concatenate them in a channel dimension, which can be formulated as:

$$\mathbf{g}_t = [\mathbf{f}_t(1); \mathbf{f}_t(2); \dots; \mathbf{f}_t(d)], \quad (8)$$

where $[\cdot; \cdot]$ is a channel-wise concatenation operation between features, and d is the total number of selected layers. Then, we pass them to the pixel-wise MLP depth predictor, and the generalization of Eq. 7 in terms of Eq. 8 can be stated as:

$$\mathbf{d}_t = \text{MLP}(\mathbf{g}_t). \quad (9)$$

We modify the pixel-wise depth predictor by appending an additional time-embedding block to the input in order to

predict the depth map at arbitrary timesteps. Therefore, we can use this predictor throughout the entire sampling process. We follow the time-embedding module of diffusion U-Net. Applying it to Eq. 7, we can rewrite the equation as:

$$\mathbf{d}_t = \text{MLP}(\mathbf{g}_t, t). \quad (10)$$

Loss function. We train the depth estimator only with the features from the frozen diffusion U-Net and the ground-truth depth map \mathbf{y} by optimizing the L1 loss formulated as:

$$\mathcal{L}_{\text{depth}} = \|\mathbf{d}_t - \mathbf{y}\|_1. \quad (11)$$

This whole procedure allows us to achieve reasonable label-efficient prediction performance in the depth domain, as demonstrated in Fig. 4(b). The depth prediction scheme allows us to predict the depth map not only for any input images but also for the intermediate images under generation in arbitrary sampling steps, as shown in Fig. 3, since the representations of diffusion models are inherently learned with the timesteps.

4.3. Depth Guided Sampling for Diffusion Model

To ensure that the generated images yield plausible depth maps, we encourage the predicted depth maps to be accurate during the sampling process. To this end, we propose two different guidance techniques that use the representations of the denoising U-Net. Utilizing these techniques during the sampling process regularizes the model to generate images that are aware of the dense map prior. Specifically, we use the aforementioned efficiently-trained depth predictors in Sec. 4.2, which can predict the depth maps from images at any sampling steps.

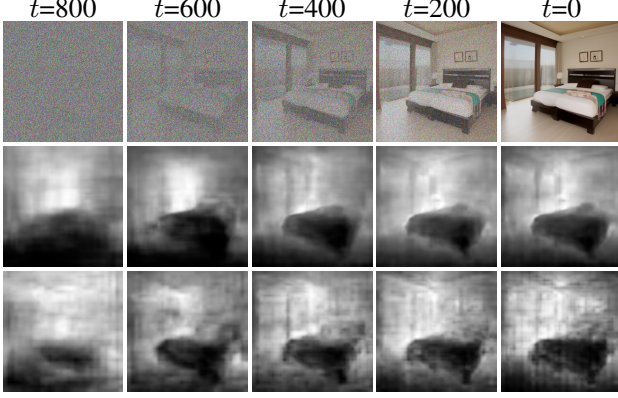


Figure 3. **Visualizations of the sampling process of our framework:** (from top to bottom) predicted images, depth predictions from the strong-branch predictor, and depth predictions from the weak-branch predictor. As exemplified, the strong-branch predictor gives robust depth predictions even at the early stage.

Unfortunately, because of the absence of a pre-determined label, we cannot compute loss using this label and cannot give guidance during the sampling process. Therefore we build two alternative loss functions that can act as guidance constraints, which we discuss in detail in the following sections. Considering Eq. 6, The general form of guidance equation is formulated by:

$$\mathbf{x}_{t-1} \sim \mathcal{N}(\mu_{\theta}(\mathbf{x}_t) - \omega \nabla_{\mathbf{x}_t} \mathcal{L}_{\text{depth}}, \Sigma_{\theta}(\mathbf{x}_t)). \quad (12)$$

Depth consistency guidance. One naive approach for providing depth guidance to the images in the absence of ground truth depth information is pseudo-labeling [29, 51], but it is challenging to generate a confident prediction that can be pseudo-label. Our first guidance method is inspired by FixMatch [51], which leverages both pseudo-labeling [29] and consistency regularization methods [2, 45]. It boosts performance by considering the weakly-augmented labels as pseudo-label. Our hypothesis derives from this design: we argue that the richer the representation is, the more faithful produced depth map becomes. Therefore, we regard the predictions from the aggregation of more feature blocks to be more informative, which makes them suitable to be treated as robust predictions (Fig. 3), i.e., pseudo-labels. We call such predictions, which use multiple feature blocks, strong branch predictions, and those that utilize relatively fewer features weak branch predictions.

In specific, we use the features $\mathbf{g}^W = [\mathbf{f}_t(6)]$ for weak branch features, and $\mathbf{g}^S = [\mathbf{f}_t(2); \mathbf{f}_t(4); \mathbf{f}_t(5); \mathbf{f}_t(6); \mathbf{f}_t(7)]$ for strong branch features. To account for the different channel dimensions of these two aggregated features, we design two asymmetric predictors: MLP-S and MLP-W. The first predictor receives more features from the U-Net block, while the second one receives fewer features, and we train them together. We feed the collected features to these

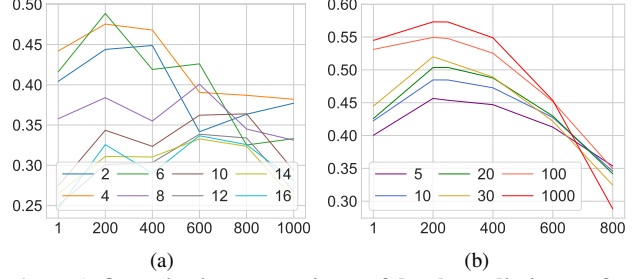


Figure 4. **Quantitative comparisons of depth prediction performance.** Evaluation of depth estimation performance for varying timesteps according to different U-Net blocks and the number of training images. The x-axis denotes timesteps and the y-axis denotes the accuracy of depth estimation. (a) Comparison of depth prediction accuracy according to different U-Net blocks. Each line denotes the layer from which the feature map is extracted in the decoder of U-Net. (b) Comparison of depth prediction accuracy with the number of images shown in training. For (b), each line denotes the number of samples shown.

MLPs and obtain the depth map predictions:

$$\mathbf{d}_t^S = \text{MLP-S}(\mathbf{g}_t^S, t), \quad \mathbf{d}_t^W = \text{MLP-W}(\mathbf{g}_t^W, t). \quad (13)$$

As stated above, we treat \mathbf{d}_t^S as a pseudo-label and \mathbf{d}_t^W as a prediction then compute the loss using a consistency loss between two predicted dense maps. We apply the stop-gradient operation to the strong features, preventing the strong prediction from learning the weak prediction [6, 51]. The gradient of the loss with respect to \mathbf{x} flows through the diffusion U-Net and guides the sampling process as done in [8]. This process can be formulated as

$$\mathcal{L}_{\text{dc}} = \|\text{stopgrad}(\mathbf{d}_t^S) - \mathbf{d}_t^W\|_2^2, \quad (14)$$

where stopgrad denotes the stop-gradient operation.

Finally, we can guide the generation process by using this gradient with Eq. 12, and it can be formulated as:

$$\mathbf{x}_{t-1} \sim \mathcal{N}(\mu_{\theta}(\mathbf{x}_t) - \omega_{\text{dc}} \nabla_{\mathbf{x}_t} \mathcal{L}_{\text{dc}}, \Sigma_{\theta}(\mathbf{x}_t)), \quad (15)$$

where ω_{dc} denotes the guidance scale.

Depth prior guidance. We also propose another guidance method, which we call depth prior guidance, to inject depth prior into the sampling process. The pretrained diffusion model can effectively refine the noised distributions to realistic distributions [34], or it can help to optimize the noised initialization of the data to match with the real data by utilizing the knowledge of the diffusion model [17]. Therefore we train another small-resolution diffusion U-Net ϵ_{ϕ} on the depth domain and use it as our prior for the second guidance method. As described in Sec. 4.2, we can extract the features from the decoder part of the image-generating U-Net to estimate the corresponding depth map using MLP

depth predictor. Utilizing the prior diffusion model, we inject noise to the depth prediction \mathbf{d}_0^S using a forward process of diffusion like:

$$\mathbf{d}_\tau^L = \sqrt{\alpha_\tau} \mathbf{d}_0^S + \sqrt{1 - \alpha_\tau} \eta, \quad \eta \sim \mathcal{N}(\mathbf{0}, \mathbf{I}), \quad (16)$$

where τ is the timestep that is used in a prior diffusion model. After adding noise to the depth prediction, we feed it to our prior network to estimate the added noise. Then we calculate the gradient of the mean-squared error between the added noise and the predicted noise concerning x . This process is then defined as:

$$\mathcal{L}_{dp} = \|\eta - \epsilon_\phi(\mathbf{d}_\tau^S)\|_2^2. \quad (17)$$

Treating the gradient of the above loss as an external classifier gradient like [8], we can guide the generated image to match with the depth prior like:

$$\mathbf{x}_{t-1} \sim \mathcal{N}(\mu_\theta(\mathbf{x}_t) - \omega_{dp} \nabla_{\mathbf{x}_t} \mathcal{L}_{dp}, \Sigma_\theta(\mathbf{x}_t)), \quad (18)$$

where ω_{dp} denotes the guidance scale.

Overall guidance. By integrating the proposed depth consistency guidance and depth prior guidance, we can guide the sampled image using both. Using Eq. 15 and 18, our overall sampling can be written as:

$$\mathbf{x}_{t-1} \sim \mathcal{N}(\mu_\theta(\mathbf{x}_t) - \omega_{dc} \nabla_{\mathbf{x}_t} \mathcal{L}_{dc} - \omega_{dp} \nabla_{\mathbf{x}_t} \mathcal{L}_{dp}, \Sigma_\theta(\mathbf{x}_t)). \quad (19)$$

5. Experiments

5.1. Experimental Settings

Datasets. We use LSUN-Bedroom and LSUN-Church [64] datasets for both depth estimation tasks and image generation tasks and demonstrate depth-aware image synthesis in indoor scenes and outdoor scenes, respectively. Since there are no ground-truth depth labels in the LSUN dataset, we generate pseudo-labels using a DPT [39] pretrained on NYU-Depth dataset [49] and utilize them for training the depth estimator.

Implementation details. We conduct our experiment based on [4], where we modify the architecture of the pixel classifier to the depth estimator. We use the pretrained weights from ADM [8] for LSUN-Bedroom, and for the LSUN-Church dataset, we build upon the public repository of DDIM [52] and Diffusers library [59]. We use Adam optimizer [25] to train the depth predictor MLP, and for the sampling of the diffusion model, we use a DDIM [52] sampler with a DDIM25 scheduler provided by the official repository of ADM [8] and DDIM. More detailed hyperparameters and settings are shown in supplementary materials.

Evaluation metrics. We evaluate our generation results using the following [8] quality metrics: Fréchet Inception Distance (FID) [19], Inception Score (IS) [46], and Precision & Recall Score [26]. For the depth evaluation, we use accuracy under the threshold ($\delta < 1.25$) and absolute relative error (AbsRel).

Evaluation metrics for depth-awareness. The performance metrics used in the image domain do not account for geometric awareness, which is the main contribution of our work. Therefore, we introduce a novel performance metric for models that generate depth-guided images. First, we predict the depth maps of generated images using Dense Prediction Transformer (DPT) [39], a state-of-the-art monocular depth estimator. To measure the reality of the depth estimation map, we directly evaluate FID [48] with depth images denoted dFID. To make a fair comparison, we build the reference batch following [8] with the depth predictions of images from the dataset with DPT-Hybrid.

5.2. Experimental Results

Depth prediction performance. First, to guide the diffusion sampling process using the depth predictor, we must validate its performance according to varying training dataset sizes, feature blocks, and timesteps. To give guidance for synthesizing images for almost all timesteps, we train the predictor for timesteps $t < 800$. This is due to our observation that the depth predictions at $t \geq 800$ do not have any useful information. We evaluate the depth performance using the depth accuracy metric, and the results are shown in Fig. 4. Based on the results in Fig. 4 (a), we choose to use the middle feature blocks $\{l_n\} = \{2, 4, 5, 6, 7\}$, which show relatively high accuracy. In DCG, we also choose the feature maps by sorting the layer by accuracy, and the result is $S = \{2, 4, 5, 6, 7\}$ and $W = \{6\}$. Next, Fig. 4 (b) shows the depth prediction accuracy with the number of training images and the evaluated timesteps. We report the mean from a total of 10-fold training results to reduce the sampling variance. As the training data size increases, the performance of the model shows improvement as well. When trained with 1,000 images, the model achieves the highest accuracy. However, the performance increase compared to the 100-label setting is marginal, so we choose to use 100 images for training the depth predictor.

Quantitative results. We compare the results of evaluation metrics for LSUN-Bedroom between unguided ADM [8] and ADM with our guidance, and the results are shown in Tab. 1. Compared to our baseline, ADM guided by DPG or DCG shows performance improvement on dFID, the evaluation metric of the depth domain. Meanwhile, our results are still comparable to traditional quality measures

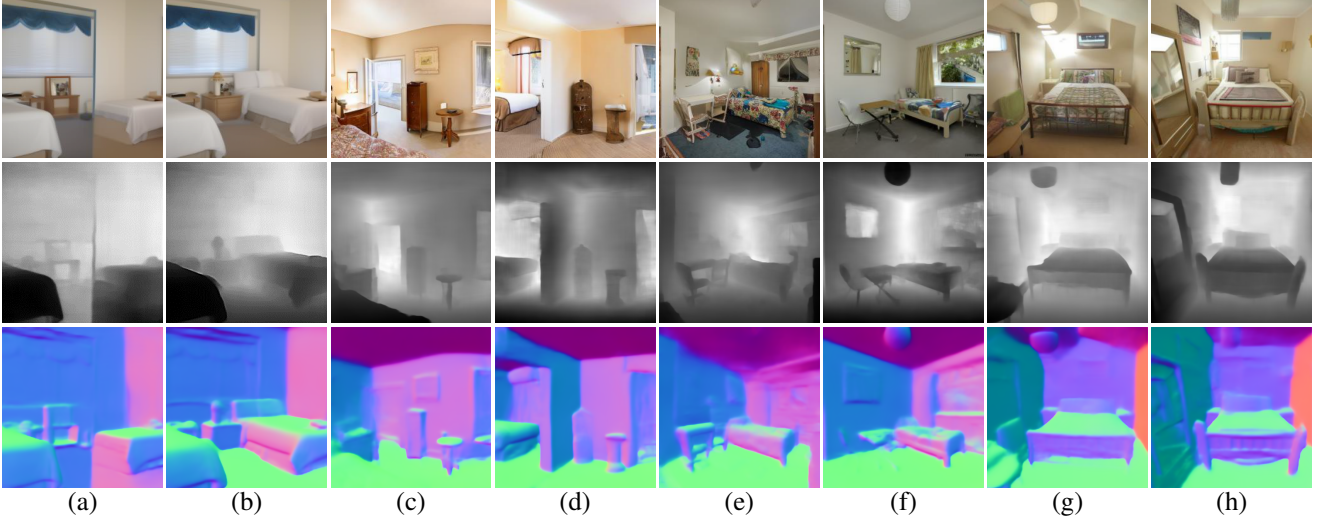


Figure 5. **Qualitative comparison on LSUN bedroom datasets [64].** We visualize (top) the samples without guidance ((a), (c), (e), (g)) and with depth-aware guidance ((b), (d), (f), (h)), and their corresponding depths [39] (middle) and surface normals [3] (bottom).

Methods	DPG	DCG	dFID (\downarrow)	FID (\downarrow)	IS (\uparrow)	Precision (\uparrow)	Recall (\uparrow)
Baseline	-	-	15.71	6.72	2.39	0.57	0.53
DAG	✓	-	<u>14.18</u>	<u>6.80</u>	2.42	<u>0.56</u>	0.54
	-	✓	15.27	7.25	<u>2.51</u>	<u>0.56</u>	<u>0.56</u>
	✓	✓	13.93	7.59	2.58	0.53	0.57

Table 1. **Quantitative Results of the baseline and ours.** dFID denotes the FID score using the estimated depth image. The metrics are computed with 5,000 generated samples. Best results are in bold, while the second best are underlined.

like FID. It can be interpreted that there is a trade-off between structure awareness and texture quality. We also evaluate the performance of our guidance method on LSUN-Church [64] dataset using the same metrics above, and the results are shown in Tab. 2. Generated samples by using our method report better performance in depth-aware metrics like dFID.

Qualitative results. In addition, we compare the result from ADM [8] without our guidance and with our guidance method in Fig. 5. We show both generated images and predicted depth maps using DPT [39], which demonstrates the effectiveness of our method of generating depth-aware images so that depth prediction models can predict the depth more robustly. Unlike guidance-free sampling, which is shown to generate geometrically implausible results, our method successfully generates depth-aware samples. Moreover, we represent surface normal estimation [3] (Fig. 5) and point cloud visualization (Fig. 6) to show the effectiveness in 3D scene understanding. The predictions made by our method show clearer boundaries and contain high-level details in scene geometry.

We also provide qualitative comparisons on LSUN-Church [64] between unguided samples and samples using our guidance method in Fig. 7. Similar to the results of

Methods	DPG	DCG	dFID (\downarrow)	FID (\downarrow)
Baseline	-	-	17.69	17.51
DAG	✓	-	17.43	18.14
	-	✓	17.40	19.75
	✓	✓	17.31	20.01

Table 2. **Quantitative results on the LSUN-church [64] datasets.**

LSUN-Bedroom, we find that our guidance method can effectively preserve geometric characteristics.

5.3. Ablation Study

For our ablation study, we analyze the effectiveness of different experimental settings and choices in our framework. To reduce the effect of random variation, we fix the random seed so that all variants see the same images in the same order. To compute the metrics, We conduct all ablation studies on 1,000 generated samples.

Guidance scale. We study the relationship between the guidance scale and image quality in terms of FID and dFID, for each DCG and DPG. Fig. 8 shows the tendency of the metrics versus scales of each guidance. As depicted in Fig. 8, DCG and DPG obtains the best results at $\omega_{dc} = 40$



Figure 6. **Visualization of point cloud representation obtained by depth information.** We compare the results generated from the baseline without (top) and with (bottom) our guidance by showing images and transforming them into point cloud visualizations in four different views.

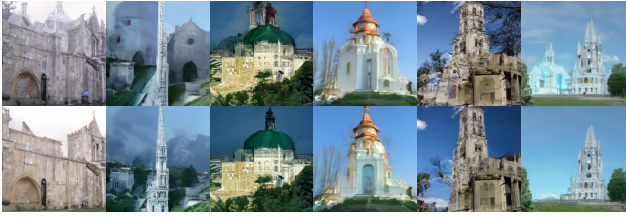


Figure 7. **Qualitative results on LSUN-church [64] dataset.** First row is unguided samples from DDIM [52], and the second row is guided samples using our guidance method, called depth-aware guidance (DAG).

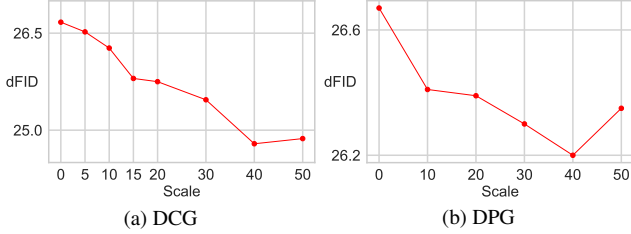


Figure 8. **Comparison of dFID with respect to the guidance scales of DCG and DPG.**

Method	dFID (\downarrow)	FID (\downarrow)
Baseline	26.77	18.24
32×32	25.14	19.86
64×64	25.96	18.85
128×128	25.07	21.69

Table 3. **Ablation study of the resolution of the prior network.**

and $\omega_{dp} = 40$ in dFID, respectively. Therefore, we treat this scale as default for the remaining part.

Resolution of the prior network. In our second guidance method, DPG, we need to train a diffusion network to give a prior for condition image. But there are limitations in computation cost for the sampling process, so we choose the proper model size for the prior diffusion network. As our output depth map has a resolution of 64×64 , we interpolate the depth map when fed to the prior network. We test

Method	$\delta > 1.25$ (\uparrow)	AbsRel. (\downarrow)
Supervised	79.06	0.144
Unguided data	72.55	0.185
DAG-based data	77.54	0.151

Table 4. **Application for depth estimation.** We train the depth estimation model from scratch using U-Net [41] based backbone network with our synthesized data.

three resolutions: $[32 \times 32, 64 \times 64, 128 \times 128]$ for the pre-trained prior diffusion network, and the quantitative results are shown in Tab. 3. The 128×128 outperforms the other resolution settings in all metrics we calculated.

5.4. Application for Depth Estimation

To improve the effects of our generation as unlabeled data, we leverage the guided images and corresponding depth maps. We train the U-Net-based depth estimation network [14] and evaluate the metrics with the NYU-Depth datasets [49]. We compare the training results using reference data, unguided generated results, and our generated results. Tab. 4 shows that the images generated by DAG-based data are more helpful in training the depth predictor than the unguided samples set.

6. Conclusion

In this paper, we propose a label-efficient method for predicting depth maps of images under generation by the reverse process of diffusion model using internal representations. We also introduce a new guidance scheme to guide the image to have a reasonable depth map. In addition, to resolve the problem that existing measurement methods cannot capture these depth feasibilities, we present a new evaluation metric that effectively represents this depth awareness using pretrained depth estimation networks.

References

- [1] Emmanuel Brempontg Asiedu, Simon Kornblith, Ting Chen, Niki Parmar, Matthias Minderer, and Mohammad Norouzi. Decoder denoising pretraining for semantic segmentation. *arXiv preprint arXiv: Arxiv-2205.11423*, 2022. 1, 2, 3, 4
- [2] Philip Bachman, Ouais Alsharif, and Doina Precup. Learning with pseudo-ensembles. *Advances in neural information processing systems*, 27, 2014. 2, 5
- [3] Gwangbin Bae, Ignas Budvytis, and Roberto Cipolla. Estimating and exploiting the aleatoric uncertainty in surface normal estimation. In *Proceedings of the IEEE/CVF International Conference on Computer Vision (ICCV)*, pages 13137–13146, October 2021. 1, 7, 14
- [4] Dmitry Baranchuk, Andrey Voynov, Ivan Rubachev, Valentin Khruikov, and Artem Babenko. Label-efficient semantic segmentation with diffusion models. In *International Conference on Learning Representations*, 2022. 1, 2, 3, 4, 6
- [5] Shariq Farooq Bhat, Ibraheem Alhashim, and Peter Wonka. Adabins: Depth estimation using adaptive bins. In *CVPR*, pages 4009–4018, 2021. 3
- [6] Xinlei Chen and Kaiming He. Exploring simple siamese representation learning. In *Proceedings of the IEEE/CVF Conference on Computer Vision and Pattern Recognition*, pages 15750–15758, 2021. 5
- [7] Jooyoung Choi, Sungwon Kim, Yonghyun Jeong, Youngjune Gwon, and Sungroh Yoon. Ilvr: Conditioning method for denoising diffusion probabilistic models. *arXiv preprint arXiv:2108.02938*, 2021. 2
- [8] Prafulla Dhariwal and Alexander Nichol. Diffusion models beat gans on image synthesis. *Advances in Neural Information Processing Systems*, 34:8780–8794, 2021. 1, 2, 3, 5, 6, 7, 12
- [9] Alexey Dosovitskiy, Lucas Beyer, Alexander Kolesnikov, Dirk Weissenborn, Xiaohua Zhai, Thomas Unterthiner, Mostafa Dehghani, Matthias Minderer, Georg Heigold, Sylvain Gelly, et al. An image is worth 16x16 words: Transformers for image recognition at scale. *arXiv preprint arXiv:2010.11929*, 2020. 3
- [10] David Eigen, Christian Puhrsch, and Rob Fergus. Depth map prediction from a single image using a multi-scale deep network. *Advances in neural information processing systems*, 27, 2014. 3
- [11] Patrick Esser, Robin Rombach, and Björn Ommer. Taming transformers for high-resolution image synthesis, 2020. 2
- [12] Hany Farid. Perspective (in) consistency of paint by text. *arXiv preprint arXiv:2206.14617*, 2022. 3
- [13] Huan Fu, Mingming Gong, Chaohui Wang, Kayhan Batmanghelich, and Dacheng Tao. Deep ordinal regression network for monocular depth estimation. In *CVPR*, pages 2002–2011, 2018. 3
- [14] Clément Godard, Oisín Mac Aodha, Michael Firman, and Gabriel J Brostow. Digging into self-supervised monocular depth estimation. In *Proceedings of the IEEE/CVF International Conference on Computer Vision*, pages 3828–3838, 2019. 8
- [15] Ian Goodfellow, Jean Pouget-Abadie, Mehdi Mirza, Bing Xu, David Warde-Farley, Sherjil Ozair, Aaron Courville, and Yoshua Bengio. Generative adversarial nets. *Advances in neural information processing systems*, 27, 2014. 3
- [16] Ian Goodfellow, Jean Pouget-Abadie, Mehdi Mirza, Bing Xu, David Warde-Farley, Sherjil Ozair, Aaron Courville, and Yoshua Bengio. Generative adversarial networks. *Communications of the ACM*, 63(11):139–144, 2020. 1
- [17] Alexandros Graikos, Nikolay Malkin, Nebojsa Jojic, and Dimitris Samaras. Diffusion models as plug-and-play priors. *arXiv preprint arXiv:2206.09012*, 2022. 2, 5
- [18] Shuyang Gu, Dong Chen, Jianmin Bao, Fang Wen, Bo Zhang, Dongdong Chen, Lu Yuan, and Baining Guo. Vector quantized diffusion model for text-to-image synthesis. In *Proceedings of the IEEE/CVF Conference on Computer Vision and Pattern Recognition*, pages 10696–10706, 2022. 2
- [19] Martin Heusel, Hubert Ramsauer, Thomas Unterthiner, Bernhard Nessler, and Sepp Hochreiter. Gans trained by a two time-scale update rule converge to a local nash equilibrium. *Advances in neural information processing systems*, 30, 2017. 2, 6
- [20] Jonathan Ho, Ajay Jain, and Pieter Abbeel. Denoising diffusion probabilistic models. *Advances in Neural Information Processing Systems*, 33:6840–6851, 2020. 1, 2, 3
- [21] Jonathan Ho and Tim Salimans. Classifier-free diffusion guidance. In *NeurIPS 2021 Workshop on Deep Generative Models and Downstream Applications*, 2021. 2
- [22] Susung Hong, Gyuseong Lee, Wooseok Jang, and Seungryong Kim. Improving sample quality of diffusion models using self-attention guidance. *arXiv preprint arXiv:2210.00939*, 2022. 2
- [23] Bahjat Kavar, Michael Elad, Stefano Ermon, and Jiaming Song. Denoising diffusion restoration models. *arXiv preprint arXiv:2201.11793*, 2022. 1
- [24] Seungryong Kim, Kihong Park, Kwanghoon Sohn, and Stephen Lin. Unified depth prediction and intrinsic image decomposition from a single image via joint convolutional neural fields. In *ECCV*, pages 143–159, 2016. 3
- [25] Diederik P Kingma and Jimmy Ba. Adam: A method for stochastic optimization. *arXiv preprint arXiv:1412.6980*, 2014. 6
- [26] Tuomas Kynkäänniemi, Tero Karras, Samuli Laine, Jaakko Lehtinen, and Timo Aila. Improved precision and recall metric for assessing generative models. *Advances in Neural Information Processing Systems*, 32, 2019. 6
- [27] Iro Laina, Christian Rupprecht, Vasileios Belagiannis, Federico Tombari, and Nassir Navab. Deeper depth prediction with fully convolutional residual networks. In *3DV*, pages 239–248. IEEE, 2016. 3
- [28] Samuli Laine and Timo Aila. Temporal ensembling for semi-supervised learning. *arXiv preprint arXiv:1610.02242*, 2016. 2
- [29] Dong-Hyun Lee et al. Pseudo-label: The simple and efficient semi-supervised learning method for deep neural networks. In *Workshop on challenges in representation learning, ICML*, volume 3, page 896, 2013. 5
- [30] Jin Han Lee, Myung-Kyu Han, Dong Wook Ko, and Il Hong Suh. From big to small: Multi-scale local planar guidance for monocular depth estimation. *arXiv*, 2019. 3

- [31] Bo Li, Chunhua Shen, Yuchao Dai, Anton Van Den Hengel, and Mingyi He. Depth and surface normal estimation from monocular images using regression on deep features and hierarchical crfs. In *Proceedings of the IEEE conference on computer vision and pattern recognition*, pages 1119–1127, 2015. [3](#)
- [32] Zhenyu Li, Zehui Chen, Xianming Liu, and Junjun Jiang. Depthformer: Exploiting long-range correlation and local information for accurate monocular depth estimation. *arXiv preprint arXiv:2203.14211*, 2022. [3](#)
- [33] Dahua Lin, Sanja Fidler, and Raquel Urtasun. Holistic scene understanding for 3d object detection with rgb-d cameras. In *Proceedings of the IEEE international conference on computer vision*, pages 1417–1424, 2013. [3](#)
- [34] Chenlin Meng, Yutong He, Yang Song, Jiaming Song, Jiajun Wu, Jun-Yan Zhu, and Stefano Ermon. Sdedit: Guided image synthesis and editing with stochastic differential equations. In *International Conference on Learning Representations*, 2021. [5](#)
- [35] Pushmeet Kohli, Nathan Silberman, Derek Hoiem, and Rob Fergus. Indoor segmentation and support inference from rgb-d images. In *ECCV*, 2012. [2](#)
- [36] Alex Nichol, Prafulla Dhariwal, Aditya Ramesh, Pranav Shyam, Pamela Mishkin, Bob McGrew, Ilya Sutskever, and Mark Chen. Glide: Towards photorealistic image generation and editing with text-guided diffusion models. *arXiv preprint arXiv:2112.10741*, 2021. [1](#), [2](#)
- [37] Alexander Quinn Nichol and Prafulla Dhariwal. Improved denoising diffusion probabilistic models. In *International Conference on Machine Learning*, pages 8162–8171. PMLR, 2021. [1](#), [2](#), [3](#)
- [38] Aditya Ramesh, Prafulla Dhariwal, Alex Nichol, Casey Chu, and Mark Chen. Hierarchical text-conditional image generation with clip latents. *arXiv preprint arXiv:2204.06125*, 2022. [1](#), [2](#)
- [39] René Ranftl, Alexey Bochkovskiy, and Vladlen Koltun. Vision transformers for dense prediction. In *Proceedings of the IEEE/CVF International Conference on Computer Vision*, pages 12179–12188, 2021. [1](#), [3](#), [6](#), [7](#), [12](#)
- [40] Robin Rombach, Andreas Blattmann, Dominik Lorenz, Patrick Esser, and Björn Ommer. High-resolution image synthesis with latent diffusion models. In *Proceedings of the IEEE/CVF Conference on Computer Vision and Pattern Recognition*, pages 10684–10695, 2022. [1](#), [2](#)
- [41] Olaf Ronneberger, Philipp Fischer, and Thomas Brox. U-net: Convolutional networks for biomedical image segmentation. In *International Conference on Medical image computing and computer-assisted intervention*, pages 234–241. Springer, 2015. [8](#)
- [42] Chitwan Saharia, William Chan, Huiwen Chang, Chris Lee, Jonathan Ho, Tim Salimans, David Fleet, and Mohammad Norouzi. Palette: Image-to-image diffusion models. In *ACM SIGGRAPH 2022 Conference Proceedings*, pages 1–10, 2022. [1](#)
- [43] Chitwan Saharia, William Chan, Saurabh Saxena, Lala Li, Jay Whang, Emily Denton, Seyed Kamyar Seyed Ghasemipour, Burcu Karagol Ayan, S Sara Mahdavi, Rapha Gontijo Lopes, et al. Photorealistic text-to-image diffusion models with deep language understanding. *arXiv preprint arXiv:2205.11487*, 2022. [2](#)
- [44] Chitwan Saharia, Jonathan Ho, William Chan, Tim Salimans, David J Fleet, and Mohammad Norouzi. Image super-resolution via iterative refinement. *IEEE Transactions on Pattern Analysis and Machine Intelligence*, 2022. [1](#)
- [45] Mehdi Sajjadi, Mehran Javanmardi, and Tolga Tasdizen. Regularization with stochastic transformations and perturbations for deep semi-supervised learning. *Advances in neural information processing systems*, 29, 2016. [2](#), [5](#)
- [46] Tim Salimans, Ian Goodfellow, Wojciech Zaremba, Vicki Cheung, Alec Radford, and Xi Chen. Improved techniques for training gans. *Advances in neural information processing systems*, 29, 2016. [2](#), [6](#)
- [47] Junyoung Seo, Gyuseong Lee, Seokju Cho, Jiyoung Lee, and Seungryong Kim. Midms: Matching interleaved diffusion models for exemplar-based image translation. *arXiv preprint arXiv:2209.11047*, 2022. [2](#)
- [48] Zifan Shi, Yujun Shen, Jiapeng Zhu, Dit-Yan Yeung, and Qifeng Chen. 3d-aware indoor scene synthesis with depth priors. *arXiv preprint arXiv:2202.08553*, 2022. [6](#)
- [49] Nathan Silberman, Derek Hoiem, Pushmeet Kohli, and Rob Fergus. Indoor segmentation and support inference from rgb-d images. In *European conference on computer vision*, pages 746–760. Springer, 2012. [6](#), [8](#), [12](#)
- [50] Jascha Sohl-Dickstein, Eric Weiss, Niru Maheswaranathan, and Surya Ganguli. Deep unsupervised learning using nonequilibrium thermodynamics. In *International Conference on Machine Learning*, pages 2256–2265. PMLR, 2015. [1](#), [2](#), [3](#)
- [51] Kihyuk Sohn, David Berthelot, Nicholas Carlini, Zizhao Zhang, Han Zhang, Colin A Raffel, Ekin Dogus Cubuk, Alexey Kurakin, and Chun-Liang Li. Fixmatch: Simplifying semi-supervised learning with consistency and confidence. *NIPS*, 33:596–608, 2020. [5](#)
- [52] Jiaming Song, Chenlin Meng, and Stefano Ermon. Denoising diffusion implicit models. In *International Conference on Learning Representations*, 2021. [2](#), [6](#), [8](#), [12](#)
- [53] Yang Song, Jascha Sohl-Dickstein, Diederik P Kingma, Abhishek Kumar, Stefano Ermon, and Ben Poole. Score-based generative modeling through stochastic differential equations. *arXiv preprint arXiv:2011.13456*, 2020. [2](#)
- [54] Christian Szegedy, Vincent Vanhoucke, Sergey Ioffe, Jonathon Shlens, and Zbigniew Wojna. Rethinking the inception architecture for computer vision. *arXiv preprint arXiv: Arxiv-1512.00567*, 2015. [12](#)
- [55] Keisuke Tateno, Federico Tombari, Iro Laina, and Nassir Navab. Cnn-slam: Real-time dense monocular slam with learned depth prediction. In *Proceedings of the IEEE conference on computer vision and pattern recognition*, pages 6243–6252, 2017. [2](#), [3](#)
- [56] Benjamin Ummenhofer, Huizhong Zhou, Jonas Uhrig, Nikolaus Mayer, Eddy Ilg, Alexey Dosovitskiy, and Thomas Brox. Demon: Depth and motion network for learning monocular stereo. In *CVPR*, pages 5038–5047, 2017.

- [57] Ashish Vaswani, Noam Shazeer, Niki Parmar, Jakob Uszkoreit, Llion Jones, Aidan N Gomez, Łukasz Kaiser, and Illia Polosukhin. Attention is all you need. *NIPS*, 30, 2017.
- [58] Pascal Vincent, Hugo Larochelle, Yoshua Bengio, and Pierre-Antoine Manzagol. Extracting and composing robust features with denoising autoencoders. In *Proceedings of the 25th International Conference on Machine learning*, pages 1096–1103, 2008. 3, 4
- [59] Patrick von Platen, Suraj Patil, Anton Lozhkov, Pedro Cuenca, Nathan Lambert, Kashif Rasul, Mishig Davaadorj, and Thomas Wolf. Diffusers: State-of-the-art diffusion models. <https://github.com/huggingface/diffusers>, 2022. 6
- [60] Tengfei Wang, Ting Zhang, Bo Zhang, Hao Ouyang, Dong Chen, Qifeng Chen, and Fang Wen. Pretraining is all you need for image-to-image translation. *arXiv preprint arXiv:2205.12952*, 2022. 2
- [61] Weilun Wang, Jianmin Bao, Wengang Zhou, Dongdong Chen, Dong Chen, Lu Yuan, and Houqiang Li. Semantic image synthesis via diffusion models. *arXiv preprint arXiv:2207.00050*, 2022. 2
- [62] Xiaolong Wang, David Fouhey, and Abhinav Gupta. Designing deep networks for surface normal estimation. In *CVPR*, pages 539–547, 2015. 3
- [63] Yan Wang, Wei-Lun Chao, Divyansh Garg, Bharath Hariharan, Mark Campbell, and Kilian Q Weinberger. Pseudolidar from visual depth estimation: Bridging the gap in 3d object detection for autonomous driving. In *Proceedings of the IEEE/CVF Conference on Computer Vision and Pattern Recognition*, pages 8445–8453, 2019. 2
- [64] Fisher Yu, Ari Seff, Yinda Zhang, Shuran Song, Thomas Funkhouser, and Jianxiong Xiao. Lsun: Construction of a large-scale image dataset using deep learning with humans in the loop. *arXiv preprint arXiv:1506.03365*, 2015. 2, 6, 7, 8, 12, 15
- [65] Qian-Yi Zhou, Jaesik Park, and Vladlen Koltun. Open3D: A modern library for 3D data processing. *arXiv:1801.09847*, 2018. 14

DAG: Depth-Aware Guidance with Denoising Diffusion Probabilistic Models

- Supplementary Materials -

In the following, we provide more qualitative results, details of our method, and further visualizations of our sampling results. Specifically, we provide additional implementation details, details on proposed metrics, hyperparameter settings, and pseudo-code for our method in Sec. 6. Next, we show various visualization such as point cloud or surface normal from samples by our method in Sec. 6. Finally, in Sec. 6, we discuss the possible limitations of our method.

A Further Details

A.1 Implementation Details

Hyperparameter Settings. We report hyperparameters used in the training of the depth estimator and sampling process in Table 5. For two datasets, LSUN-Bedroom and LSUN-Church [64], we use almost the same hyperparameters for depth estimator training. Note that we use two different U-Net implementations from ADM [8] and DDIM [52] because of the existence of pretrained weights, thus the selection of the feature extraction block is slightly changed.

	Hyperparameters	LSUN-Bedroom [64]	LSUN-Church [64]
Training	learning rate	$1e-5$	$1e-5$
	optimizer	Adam	Adam
	\mathbf{g}^W	$[\mathbf{f}_t(6)]$	$[\mathbf{f}_t(17)]$
	\mathbf{g}^S	$[\mathbf{f}_t(2); \mathbf{f}_t(4); \mathbf{f}_t(5); \mathbf{f}_t(6); \mathbf{f}_t(7)]$	$[\mathbf{f}_t(3); \mathbf{f}_t(5); \mathbf{f}_t(7); \mathbf{f}_t(9); \mathbf{f}_t(13); \mathbf{f}_t(17)]$
	Timestep Sampler	Uniform	Uniform
	Time embedding dimension	256	256
Sampling	Timestep Scheduler	25	25
		DDIM	DDIM
	τ	Uniform	Uniform
	ω_{dc}	40.0	10.0
	ω_{dp}	40.0	50.0

Table 5. **Detailed hyperparameter settings.** Training denotes hyperparameters used at the training depth estimator, and sampling denotes hyperparameters used at sampling diffusion models using DAG.

A.2 PyTorch-like Pseudo Code.

Guidance Method. We provide a detailed PyTorch-like pseudo-code of our guidance method in Algorithm 1.

Network Architecture for Depth Estimator. We use a 3-layer MLP that receives concatenated feature vector of a pixel to predict the depth map. Following the diffusion network, we apply the SiLU activation function. Detailed architecture is shown in Fig. 2 of the main paper and Algorithm 2 of this supplementary material. Also, we add a time-embedding module to this depth estimator MLP following the implementation of U-Net of ADM [8].

A.3 Proposed Metric

We propose a new metric, called dFID, which can evaluate the depth-awareness, and we describe the details of the proposed metrics in this section.

Depth FID. To compute the FID of the depth domain, we first estimate the depth map using the NYU-Depth [49] pretrained depth estimator DPT-Hybrid [39], which is available in the official repository. Then, identical to the original FID, we compute the Fréchet distance of embeddings collected from depth images using the Inception v3 model [54].

Algorithm 1 Pseudo Code of Our Depth-Aware Guidance

```
def cond_fn(img, t, y=None):
    """
    dc: scale of depth consistency guidance
    dp: scale of depth prior guidance
    """
    img = img.detach().requires_grad_(True)

    # feature extraction
    strong_feature, weak_feature = feature_extractor(img, t)

    # depth consistency loss
    strong_depth = strong_depth_predictor(strong_feature, t)
    weak_depth = weak_depth_predictor(weak_feature, t)
    dcg_loss = F.l1_loss(weak_depth, strong_depth.detach())

    # depth prior loss
    noise = torch.randn_like(strong_depth)
    t_rand = torch.randint(0, 25)

    strong_depth_t = diffusion.q_sample(strong_depth, t_rand, noise=noise)
    strong_eps = prior_diffusion_model(strong_depth_t, t_rand)
    dpq_loss = torch.mean((strong_eps - noise) ** 2)

    loss = dp * dpq_loss + dc * dcg_loss
    grad = torch.autograd.grad(loss, img, allow_unused=True)[0]

    return -1.0 * grad
```

Algorithm 2 Pseudo Code of Our Label-efficient Depth Estimator

```
class MLPBlock(nn.Module):
    def __init__(self, in_dim, out_dim,
                 time_dim):
        super().__init__()
        self.linear = nn.Linear(in_dim,
                                out_dim)
        self.is_last = True if out_dim == 1
                        else False

        if not self.is_last:
            self.act = nn.SiLU()
            self.norm = nn.BatchNorm1d(
                out_dim)
            self.time_proj = nn.Linear(
                time_dim, out_dim)
        else:
            self.act = nn.Sigmoid()
            self.norm = nn.Identity()
            self.time_proj = None

    def forward(self, x, time_emb=None):
        x = self.linear(x)
        x = self.act(x)
        x = self.norm(x)
        if not self.is_last:
            x = x + self.time_proj(time_emb)
        return x

class DepthPredictor(nn.Module):
    def __init__(self, dim):
        super().__init__()
        self.layers = nn.ModuleList([
            MLPBlock(dim, 256, time_dim=256)
            ,
            MLPBlock(256, 128, time_dim=256)
            ,
            MLPBlock(128, 1, time_dim=256),
        ])
        self.max_depth = 10.0

    def forward(self, x, timesteps=None):
        timesteps = timestep_embedding(
            timesteps, 256)

        for layer in self.layers:
            x = layer(x, timesteps)

        return x * self.max_depth
```

B More Visualizations

In Fig. 9, we additionally show more qualitative results from the baseline and our proposed guidance method. Unlike the baseline, the images generated with our guidance have little ambiguity in perspective and represent the layout robustly. We can demonstrate this by plenty of visualizations of the corresponding depth maps, where we can see diffusion models with our guidance yield more geometrically plausible results while the unguided counterparts do not.

B.1 Point Cloud Visualization

To show the depth awareness and geometric plausibility of our proposed guidance, we display additional results of the point cloud from generated images and its depth as depicted in Fig. 10. We use Open3D library [65] to construct the point clouds, and capture various viewpoints, e.g., front, left, right, and upward, to compare 3D-represented images. We can find that the guided samples show more plausible point cloud visualization and robust geometric consistency when viewed from the same viewpoint.

B.2 Surface Normal Visualization

In Fig. 11, we also demonstrate the surface normal estimation [3] results of the baseline and our proposed approach. Since surface normals are important properties of a geometric surface, we use them to look into the geometrical rationality of the generated images. Furthermore, we estimate the aleatoric uncertainty [3] by predicting the probability distribution of the per-pixel surface normal. Qualitatively, the prediction made by our method contains more clear layout and boundaries, so the uncertainty near the edge of the wall is much lower than the baseline.

C Limitations and Future Works

In this study, we focus on the sampling strategy that leads the generated image to have higher depth awareness. This strategy allows us to use generated images with more reliable and precise geometric properties in a variety of downstream tasks. Because our work is the first attempt to enable the depth awareness of image synthesis in diffusion models, comparing the performance to other previous research is challenging: we only employed pretrained diffusion models due to the high computational cost of the training procedure, and data selection was also limited. If we can train the diffusion model using indoor and outdoor scene datasets we can directly demonstrate and improve the effectiveness of our guiding technique. On the other hand, since we utilize the diffusion U-Net as part of the depth estimator, gradient computation demands backpropagation through the whole U-Net, increasing the cost of the guiding process. Another potential approach to address this challenge is to train the diffusion network using depth map conditioning and sampling with classifier-free guidance, but this requires a large amount of depth-image pairs and computational cost for the joint training compared to our method.

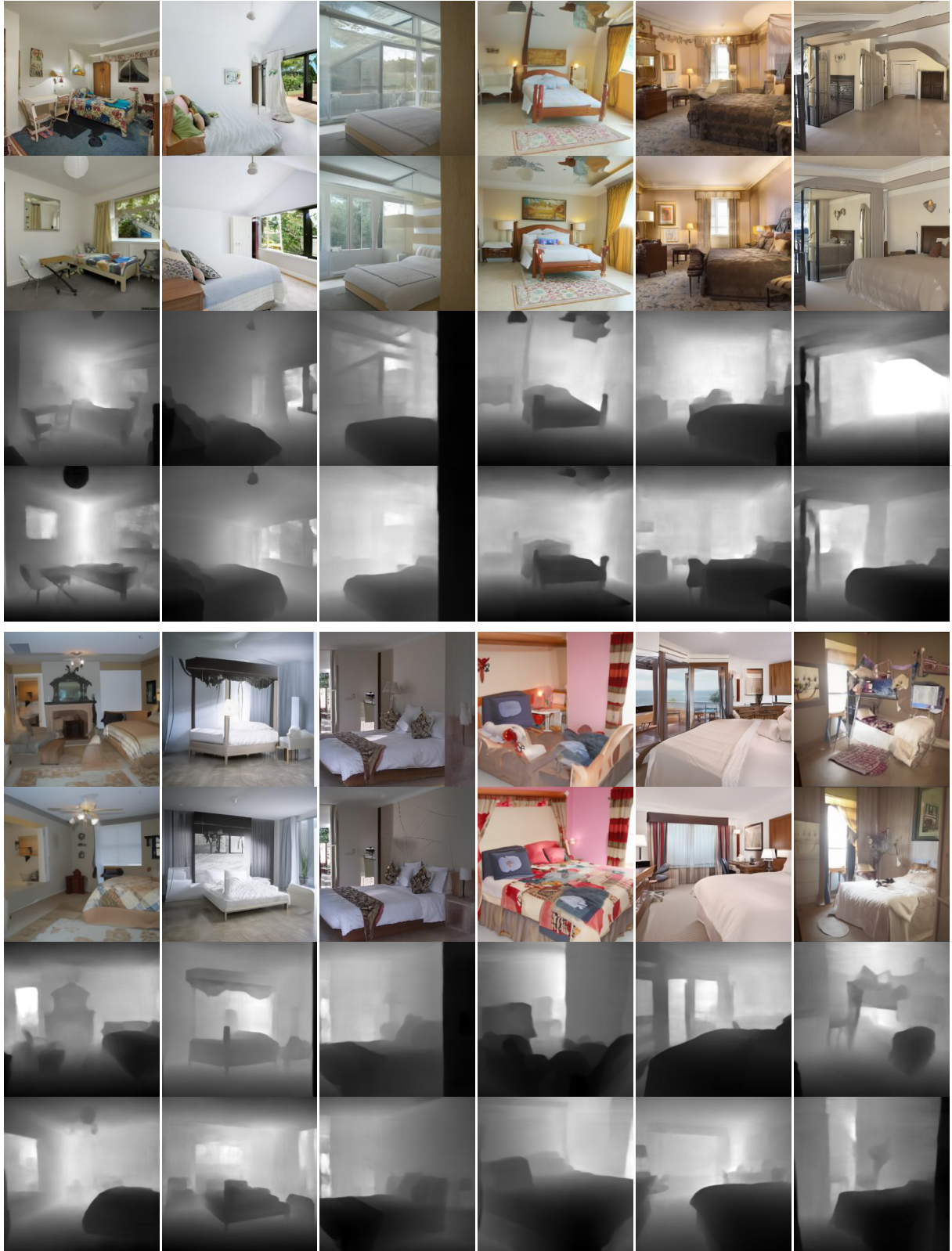


Figure 9. **Qualitative comparison on LSUN bedroom datasets** [64]. We show the results of unguided and depth-guided samples (first two rows) and their corresponding depths (last two rows).



Figure 10. **Visualization of point cloud representation obtained by depth information.** (a), (c), (e) are generated samples from ADM, and (b), (d), (f) are samples from ADM with our guidance method. The left column is generated image, and the other columns are point cloud visualizations from four different views.

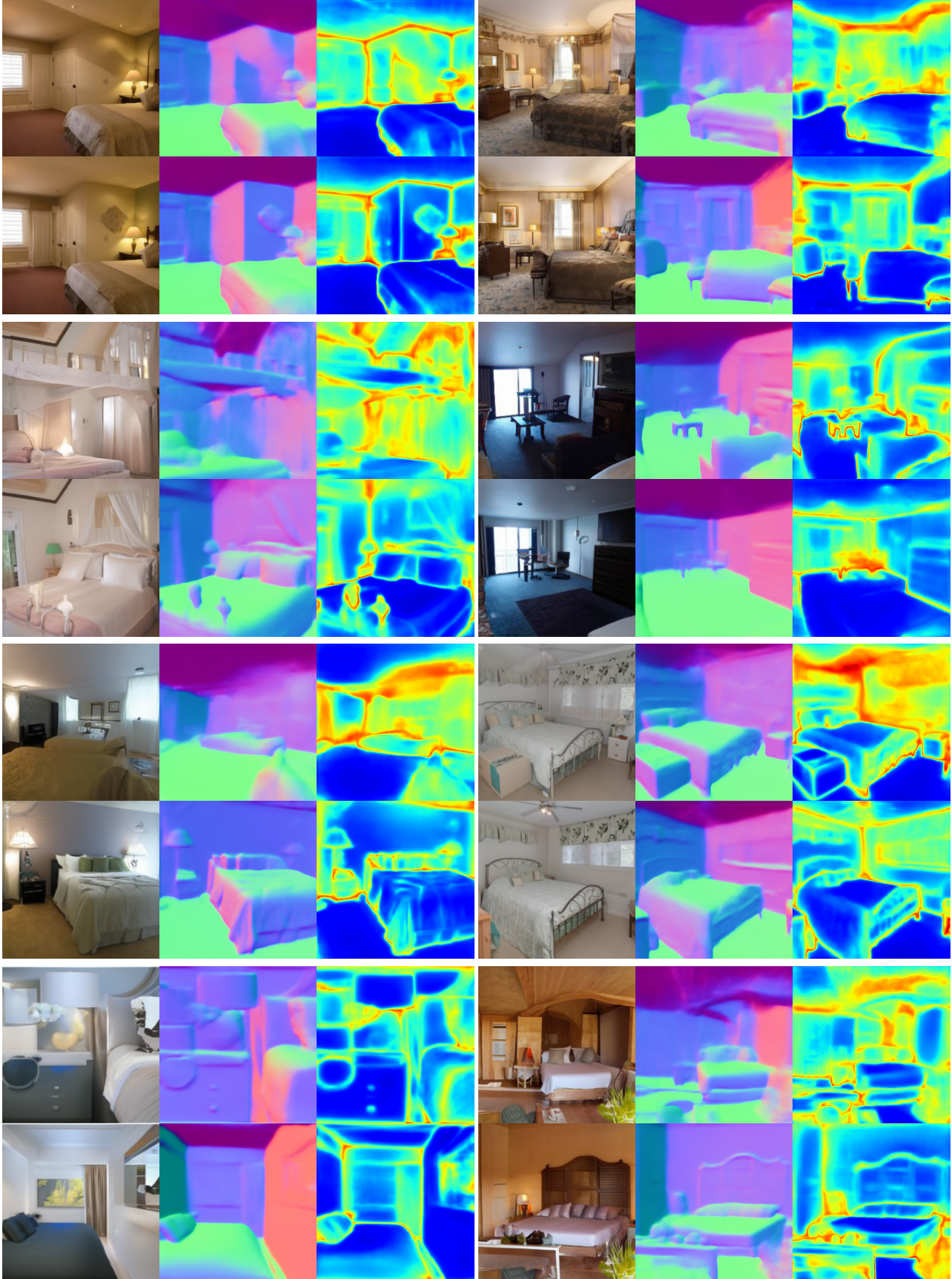


Figure 11. Qualitative comparison of the baseline and our method using surface normals and corresponding uncertainty.